Monthly Notices
of the
ROYAL ASTRONOMICAL SOCIETY

MNRAS **490,** 1283–1293 (2019)
Advance Access publication 2019 September 16

doi:10.1093/mnras/stz2597

Multifilter time-series observations of three short period ATLAS variable stars

Chris Koen★

Department of Statistics, University of the Western Cape, Private Bag X17, Cape, Bellville 7535, South Africa

Accepted 2019 September 12. Received 2019 September 5; in original form 2019 June 14

ABSTRACT

The 'Asteroid Terrestrial-impact Last Alert System' discovered hundreds of thousands of new candidate variable stars. Follow-up observations of three of these are reported in this paper. The targets were selected on the basis of having high probability of being periodic (false alarm probability for period detection smaller than 10^{-5}), short periods ($P < 0.2$ d), and being relatively bright ($g' < 17$). The targets were also chosen to be either very blue ($g' - i' < -0.4$, $r' - z' < -0.4$) or very red ($g' - i' > 2.2$, $r' - z' > 1.5$) as periodic variables with these colours are relatively rare. Two of the stars are hot subdwarfs, both of which are likely reflection effect binaries. In both cases simple models suggest that the companions may have masses very close to or below 0.1 $M_{\odot}$. The third star is also a binary, which appears to consist of two M dwarfs in a near contact configuration. At 0.12 d its period is one of the shortest known for M-type binaries.

Key words: binaries: close – stars: individual: ATO J199.6731-31.7189, LB 283, GALEX J093448.2-251248 – stars: low mass – subdwarfs – stars: variables: general.

1 INTRODUCTION

As a by-product of scanning the sky for asteroids the 'Asteroid Terrestrial-impact Last Alert System' (ATLAS) has discovered more than 300 000 strong candidates for stellar variability. The ATLAS variable star catalogue (Heinze et al. 2018), thus, provides a valuable source of interesting targets for further research. This paper presents further observations of three ATLAS periodic variables, selected for their extreme colours and short periods. The aims of this project were to obtain (i) higher signal to noise, and more densely spaced, measurements which could perhaps reveal additional periodicities, and/or finer structure not visible in the ATLAS light curves, and (ii) contemporaneous observations through several filters, which could help determine the variability mechanisms and aid in producing accurate models.

Fig. 1 is a Pan-STARRS (Chambers et al. 2016) colour–colour diagram of a sample of 3829 candidate variables extracted from the ATLAS catalogue. The stars were selected to be accessible during the observing run, to have periods short enough to be of interest ($P < 0.2$ d, see below), and be bright enough ($g' < 17$ mag) to obtain accurate photometry while cycling through filters in a few minutes. Further requirements were that the variability not be flagged as 'dubious', and that the false alarm probability for the period detected be smaller than 10^{-5}. Solid squares mark the positions of the three stars selected for observation.

There are three stars with colours slightly bluer than the two blue targets selected. Two of these are well-known hot subdwarf variables: NY Vir (e.g. Kilkenny et al. 1998) and EC 10246-2707 (Barlow et al. 2013). The third, PG 1039-119, has an ATLAS period of 0.1075 d, but is flagged as 'CBH', meaning a close binary with catalogued period being half the true period – which takes it beyond our 0.2 d limit. Finally, one object – EPIC 212540174 – is redder than the red target selected for the present study. This star was discovered by Drake et al. (2014) to be a periodic variable with $P = 0.1757$ d; those authors classified it as an ellipsoidal variable. Crossfield et al. (2018) found a period of 0.5271 d from *Kepler* observations, and reclassified the star as a contact binary. Examination of the *Kepler* light curve suggests that the star is indeed of W UMa type, but with $P = 0.1757 = 0.5271/3$ d.

Amongst the reddest stars in the ATLAS catalogue, short period binaries are of particular interest. There is a fairly sharp lower limit of about 0.2 d to the period distribution of contact binaries (e.g. Paczyński et al. 2006). Jiang et al. (2015), for example, presented a list of 10 systems with very short periods: the period of only one of these, SDSS J001641−000925, is marginally below 0.2 d ($P = 0.1986$; Davenport et al. 2013). Recent explanations for the period cut-off have been published by Jiang et al. (2012) and Stępień & Gazeas (2012), where references to earlier work can be found. The models of Stępień & Gazeas (2012), in particular, predict a minimum period close to 0.20 d. It is therefore of some interest to determine the true nature of candidate contact binaries with periods near or below this limit.

The bluest stars in the ATLAS catalogue could include variable white dwarfs and hot subdwarf stars (sdO and sdB stars). Short

★ E-mail: ckoen@uwc.ac.za

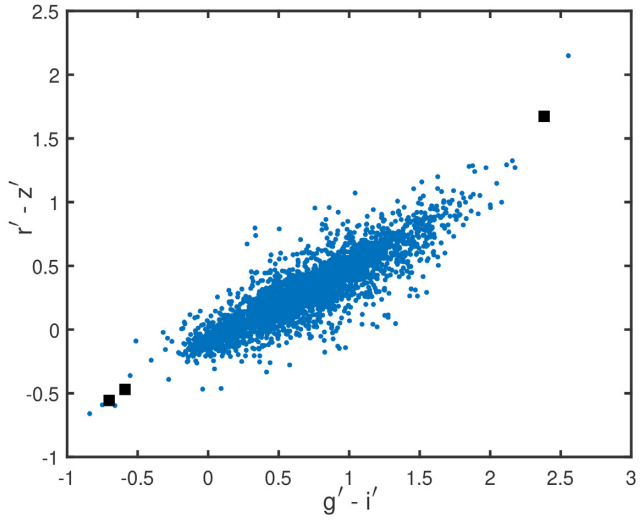

Figure 1. Colour–colour diagram of 3829 candidate periodic variables from the ATLAS catalogue. Solid squares mark the targets selected for the present study: from left to right ATO J143.7010−25.2124 (GALEX J093448.2−251248), ATO 227.2198−14.9050 (LB 283), and ATO J199.6731−31.7189.

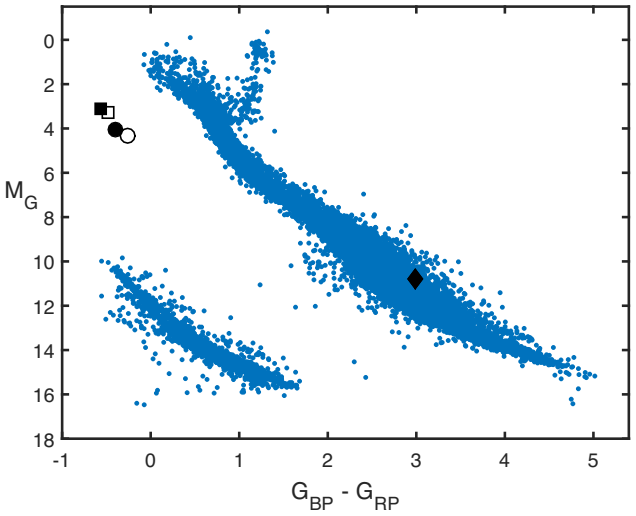

Figure 2. The positions of the three stars in a *Gaia* Hertzsprung–Russell diagram. Dots show the positions of 29 683 stars within 50 pc of earth (see fig. 6b of Gaia Collaboration 2018b). The square, circle, and diamond, respectively, show positions of *GALEX* J093448.2−251248, LB 283, and ATO J199.6731−31.7189. Open symbols denoted raw observations, filled symbols de-reddened values.

period variability could be due to either pulsation or binarity. The shortest period amongst the 3829 potential target stars is 0.04 d (∼1 h), which may be too long for most types of white dwarf pulsators except perhaps the very hot GW Vir stars (e.g. Córsico et al. 2019) or the much cooler pulsating extremely low mass white dwarfs (e.g. Calcaferro, Córsico & Althaus 2017). If the light in a binary system is dominated by a white dwarf, the intrinsic faintness of these stars implies that the companion should be either an exotic object such as a neutron star or black hole, or a cooler white dwarf (e.g. Napiwotzki et al. 2019). As far as the hot subdwarf stars are concerned, gravity mode pulsation periods are roughly 1–3 hr, but the amplitudes are low – just a few millimagnitudes (see e.g. table 5 in Koen 2011). The expectation is therefore that the extreme blue periodic variables should be binaries.

A relatively recent table of all then known binary systems containing a hot subdwarf star lists only 29 (out of 179) stars with periods shorter than 0.2 d (Kawka et al. 2015). At these short periods companion stars are white dwarfs, brown dwarfs or very cool red dwarfs. Finding further examples of $P < 0.2$ d binaries will help better characterize the short period end of the distribution, which is of importance in understanding the evolutionary routes followed by the two component stars (e.g. Kawka et al. 2015; Heber 2016).

The very red target star in Fig. 1 is ATO J199.6731−31.7189, with $(g' - r') = 1.44$, $(r' - i') = 1.68$. It is classified in the ATLAS catalogue as a close binary, with a period of 0.117 d. Phasing the ATLAS photometry with this period suggests that the star could be a contact binary with a period *below* the generally accepted lower limit. This star is discussed in detail Section 3 below.

The other two topics of this paper are ATO 227.2198−14.9050 (LB 283, EC 15061−1442) and ATO J143.7010−25.2124 (*GALEX* J093448.2−251248). Both these stars are at the extreme blue end of the spectrum – in fact, both are known to be hot subdwarf stars (Kilkenny et al. 1997; Németh, Kawka & Vennes 2012). Heber (2016) provides an extensive review of the properties of hot subdwarf stars. Discovery names (LB 283 and *GALEX* J093448.2−251248) of the two stars will be used in what follows.

LB 283 has an ATLAS variable star classification of 'Irregular' (but is none the less assigned a period of 0.1413 d), while *GALEX* J093448.2−251248 is described as a sinusoidal variable with $P = 0.125$ d.

A very recent paper by Kilkenny, Worters & Lynas-Gray (2019) shows a light curve of LB 283, sinusoidal in appearance. The authors mention that the period could be 0.075 d if the star is a reflection effect binary, or 0.15 d if it were an ellipsoidal variable. Kilkenny et al. (2019) model their white light observations as a reflection effect, finding that the secondary star is a very low mass red dwarf, which fills it Roche lobe. The multifilter observations presented below (section 4) allows us to test this finding.

He II is anomalously strong in the spectrum of *GALEX* J093448.2−251248. Németh et al. (2012) write '... the spectrum might be dominated by an sdB star and the He II line can be the signature of a hot, but faint companion.' This suggests that the star may be an ellipsoidal variable with a period of 0.25 d. Observations of *GALEX* J093448.2−251248 are discussed in Section 5. Modelling of both the subdwarf stars is performed in Section 6.

Fig. 2 locates the three stars in a Hertzsprung–Russell diagram. *Gaia* magnitudes, colours, and parallaxes were taken from Gaia Collaboration (2018a). Reddening of the nearby ATO J199.6731−31.7189 was assumed negligible, while for *GALEX* J093448.2−251248 and LB 283 values of E$(B - V)$ were taken from the literature (see below). Assuming $A_V = 3.1\mathrm{E}(B - V)$, the relations

$$A_G = 2.45E(B - V),$$
$$E(G_{\mathrm{BP}} - G_{\mathrm{RP}}) = 1.30E(B - V),$$

follow from table 3 of Wang & Chen (2019), and were used to produce the de-reddened colours and magnitudes in the figure.

Reference will be made below to various surveys: the Two Micron All Sky Survey (2MASS; Skrutskie et al. 2006), the AAVSO Photometric All-Sky Survey (APASS; e.g. Henden & Munari 2014),

Table 1. The observing log. Exposure times are in brackets after filternames. Numbers of measurements across filters are in the last column.

Starting time (HJD 2450000 +)	Filter (Exposure time) (s)				Run length (h)	*N*
			ATO J199.6731−31.7189			
8626.2081	*B* (200)	*V* (80)	*R* (30)	*I* (15)	3.3	29
8627.1915	*V* (50)	*R* (25)			3.9	110–144
8628.1987	*B* (90)				3.3	106
8629.2026	*I* (15–22)				3.3	282
			LB 283			
8623.4503	*U* (80–120)	*B* (10–30)	*V* (20–45)	*R* (45)	3.8	46–48
8628.3795	*U* (90–110)	*B* (20–30)	*V* (20)	*R* (10–45)	3.4	36–50
8629.3573	*U* (60)	*V* (15–25)			4.3	128–130
			GALEX J093448.2−251248			
8622.2810	*U* (70–120)	*B* (20)	*V* (15)	*R* (10)	2.1	31–33
8623.1908	*U* (120)	*B* (25)	*V* (15)	*R* (10)	4.3	42–44
8625.1956	*U* (80)	*B* (20)	*V* (15)	*R* (10)	4.2	69–70
8631.2189	*U* (120–160)	*B* (40)	*V* (30)	*R* (20)	1.7	20–23

the Wide-field Infrared Explorer AllWISE data release (WISE; Wright et al. 2010; Cutrie et al. 2013), the Catalina Sky Survey (CSS; Drake et al. 2014), the Panoramic Survey Telescope and Rapid Response System (Pan-STARRS; Chambers et al. 2016), and the *Gaia* astrometry mission (e.g. Gaia Collaboration 2018a). The colour index – spectral type – $T_{\rm eff}$ table http://www.pas.rochester.edu/ emamajek/EEM_dwarf_UBVIJHK_colors_Teff.txt (Pecaut, Mamajek & Bubar 2012; Pecaut & Mamajek 2013) was also freely consulted. Use of these data sources, as well as the ATLAS variable star catalogue, is gratefully acknowledged.

2 SAAO OBSERVATIONS

All observations were made with the STE4 CCD camera mounted on the 1 m telescope of the South African Astronomical Observatory (SAAO) situated at Sutherland in South Africa. The camera has a 1024 × 1024 array of pixels, covering 5 × 5 arcmin^2 of sky. Prebinning (2 × 2) was used throughout, giving a readout time of roughly 20 s. Sky conditions were variable, with some observations obtained through thin clouds and/or under bright moonlight conditions. Differentially corrected photometry was used to deal with the former problem, while the stars are bright enough, and were far enough from the moon on the sky that sky brightness was not a prohibitive problem. Seeing was generally in the approximate range 1–2 arcsec.

Observations were mostly made by cycling through either $UBVR_C$ (blue stars) or BVR_CI_C (ATO J199.6731−31.7189). However, after the first night of observing ATO J199.6731−31.7189, it was clear that, given its short period, the time resolution was insufficient with this mode of operation. Runs on this star thereafter used either one or two filters only. Exposure times were tailored to atmospheric conditions – see the log in Table 1.

Reductions were performed using an automated version of DOPHOT (Schechter, Mateo & Saha 1993). Magnitudes derived from point spread function fitting showed less scatter, and were therefore preferred. As mentioned above, magnitudes were differentially corrected, using a suite of stars in the field of view with constant, low noise light curves.

For convenience the subscripts on R_C and I_C are dropped in the rest of the paper.

3 ATO J199.6731−31.7189

Two temperature estimates for the star are available: $T_{\rm eff} = 3877$ K (*Gaia*; Andrae et al. 2018) and $T_{\rm eff} = 3218$ K (Muirhead et al. 2018). The latter estimate was derived from colour–$T_{\rm eff}$ relations for $r' - J$ and $V - J$ indices. Since there is also a variety of other photometric indices available, this is studied in more detail in the next paragraph.

Comparing $r' - i'$ and $i' - J$ colour indices (from APASS and 2MASS photometry) to the M and L dwarf tabulation by Hawley et al. (2002), suggests a spectral type of M3–4. The colour indices $B - V = 1.73$, $J - H = 0.56$, and $H - K = 0.28$ correspond to spectral types M3–M4.5 in the Pecaut & Mamajek (2013) table. The implied mass is $0.18\,{\rm M}_\odot \leq M \leq 0.36\,{\rm M}_\odot$ and the effective temperature $3100 \leq T_{\rm eff} \leq 3410$ K. From the *Gaia* parallax of 19.3 mas and the 2MASS J magnitude of 11.175, $M_J = 7.60$ which is bracketed by $M_J = 7.24$ (M3) and $M_J = 8.34$ (M4) in table 3 of Hawley et al. (2002). If it is assumed that the luminosities of the two components of ATO J199.6731−31.7189 are similar, then the absolute magnitudes of the individual stars are fainter by about 0.75 mag, which favours the M4-type. Pecaut et al. (2013) supply $M_V = 12.80$ and $M_K = 7.55$ for an M4V star; for ATO J199.6731−31.7189, we have $M_V = 12.19$ and $M_K = 6.76$, which, if adjusted by 0.75 mag, agree very well with the table values.

We conclude that the spectral type of the dominant light source in the binary is close to M4, which implies $T_{\rm eff} \approx 3200$ K, $M \approx 0.22\,{\rm M}_\odot$ for the brighter component. The result agrees well with that of Muirhead et al. (2018) mentioned above, but the temperature is ∼600K cooler than the *Gaia* value. Andrae et al. (2018) mention that for $T_{\rm eff}$ below 4000 K errors as large as 550 K can be expected in their temperature determinations; their fig. 10 furthermore suggests that the tendency might be for their temperatures to be overestimates. A further complication is that the authors derive both temperatures and reddening (put at 0.71 mag in the *Gaia G* band) from the brightness measurements in their three bandpasses (of which one has the same wavelength coverage as the other two combined). Given that values of $T_{\rm eff}$ and A_G are not independent, this may be another source of uncertainty. The shortest wavelength, and hence most reddening-sensitive, indices available for ATO J199.6731−31.7189 are $(B - V) = 1.73$ and $(g - r) = 1.44$ mag (both from APASS). These values are consistent with the M4 spectral type (see Finlator et al. 2000;

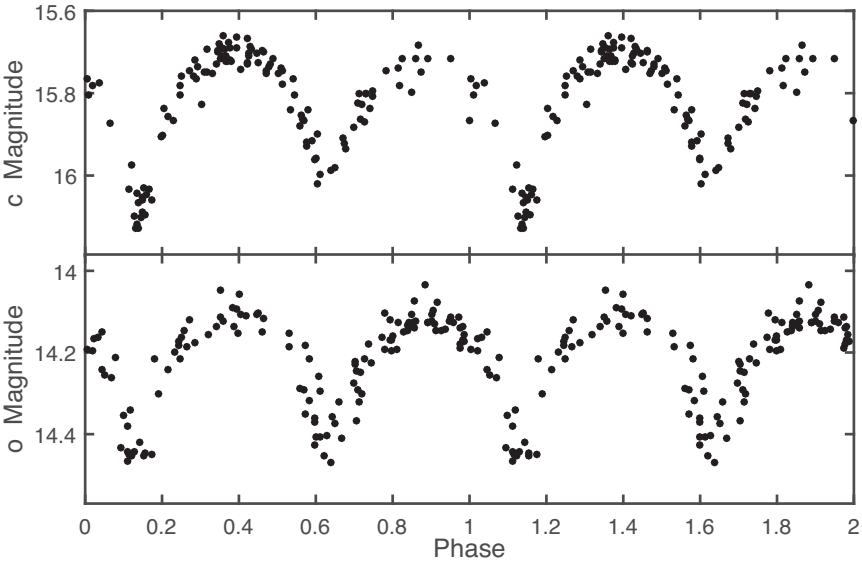

Figure 3. The ATLAS observations of ATO J199.6731−31.7189, phased with a frequency of 17.1057 d^{-1}.

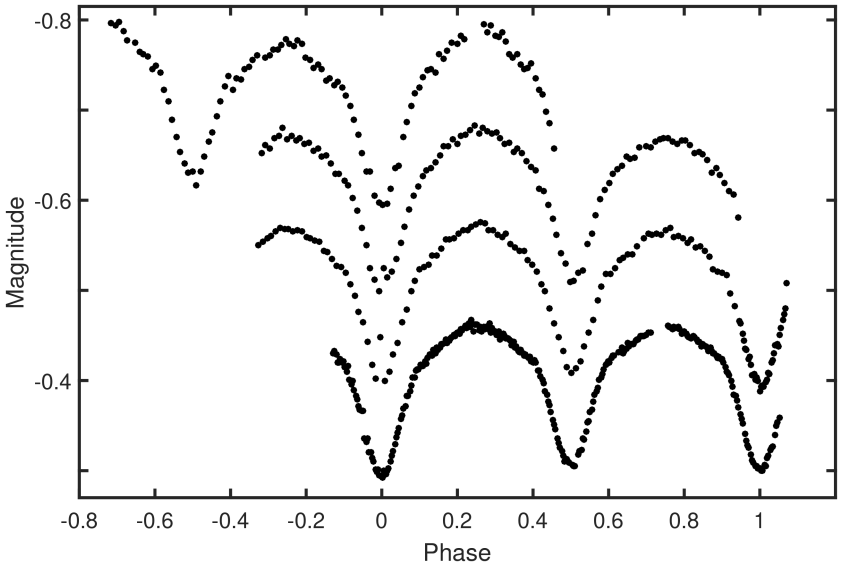

Figure 4. SAAO light curves of ATO J199.6731−31.7189. From top to bottom *B*, *V*, *R*, and *I*. Zeropoints are arbitrary.

Pecaut & Mamajek 2013) derived from the longer wavelength (and hence less reddening sensitive) indices. The implication is that there is probably very little reddening.

ATLAS observations were made through two filters denoted 'o' (orange, 560–820 nm) and 'c' (cyan, 420–650 nm). One outlier (6.2σ) was removed from the *c* data leaving 123 observations spanning 480 d. Corresponding figures for the *o* data are two outliers (3.7σ and 4.4σ), with 126 measurements spanning 543 d. Periodograms of both these data sets have substantial peaks at $f = 17.1057\ d^{-1}$ ($P = 0.058\ 46$) and harmonic frequencies. Fig. 3 shows the ATLAS data phased with a period of $2P = 0.116\ 92$ d.

The CSS covers a longer baseline (2941 d), which allows a more accurate period determination. Fitting a truncated Fourier series to 313 CSS observations of the star gives the result $P_0 = 0.116\ 920\ 41$ d with a standard error of 5.1×10^{-8} d.

Light curves obtained at SAAO are plotted in Fig. 4. It is interesting that some of the features in Fig. 3 such as the markedly different eclipse depths in the *c* data, and the apparently flat-bottomed eclipses in the *o* data, are not evident in the SAAO observations. Further observations will be required that establish whether this is due to evolution in the light curves.

The six well-observed times of primary eclipse in the SAAO data were used to estimate the ephemeris ,

$$\min(I) = 2458\,627.2298(1.03E - 4) + E \times P_0.$$

A complete binary solution awaits spectroscopic observations, but it is possible to make considerable progress with the information currently available. Inspection of the phased light curves shows the following features:

(i) Given the small difference between primary and secondary eclipses, and the modelling results discussed below, it seems likely that the two components of the binary are physically quite similar, i.e. that ATO J199.6731−31.7189 consists of two M-type stars.

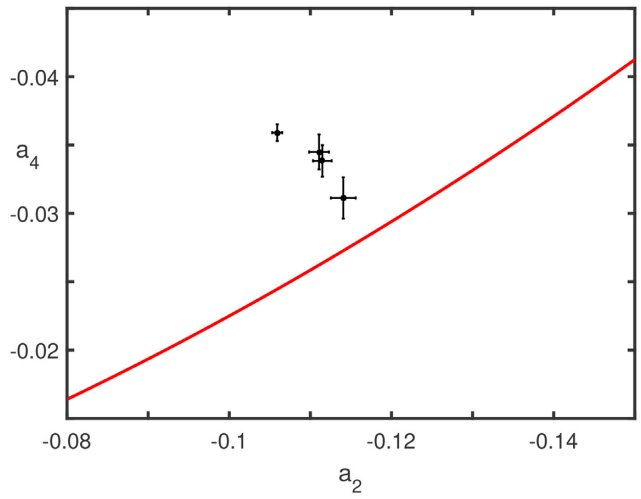

Figure 5. The first two even cosine Fourier coefficients of the light curves in Fig. 4, with error bars obtained from the least-squares fit of equation (1). From top left to bottom right *B*, *R*, *I*, and *V*. The solid line is the overcontact boundary.

(ii) There is a noticeable difference between the heights of successive maxima visible in the *B*-band light curve, and to a lesser extent in *V* and *R*. This is a well-known phenomenon in W UMa stars, referred to as the 'O'Connell effect'. To the best of the author's knowledge, there is no universally accepted explanation of the effect – see Liu & Yang (2003) for a short review.

(iii) The depth of the primary eclipse appears to be slightly variable, at least in *I*. This could be due to the presence of star-spots

(iv) There are occasional spikes in the differentially corrected light curves. The most conspicuous of these can be seen in the first *R*-band primary eclipse. There is an accompanying spike in the contemporaneous *V*-band eclipse, and a less conspicuous instance during primary eclipse ingress in *B*. It seems likely that these are short lived microflares; further observations are required to establish whether they are primarily associated with primary eclipses.

(v) The light curves can be modelled fairly accurately by the truncated Fourier series

$$F(\phi) = \mu + \sum_{k=1}^{7} [a_k \cos(2k\pi\phi) + b_k \sin(2k\pi\phi)], \quad (1)$$

where μ is the mean light level. The coefficients a_2 and a_4 can be used to crudely discriminate between contact binaries and other types of binaries; the boundary between the two types is given by

$$a_4 = a_2(0.125 - a_2),$$

(Rucinski 1997), plotted as the solid line in Fig. 5. The (a_2, a_4) pairs are slightly above this line for all four light curves, suggesting marginal to no contact.

(vi) Rucinski (1993) provided tables giving eclipse depths as a function of inclination angle i and mass ratio q. 'Depth' is defined in this context as the flux decrease during eclipse, normalized by maximum flux; values of roughly 0.3 (*B*), 0.28 (*V*), 0.27 (*R*), and 0.25 (*I*) follow from the data in Fig. 1. The $f = 0$ (marginal contact) table 4 of Rucinski (1993) then gives $64 \lesssim i \lesssim 69$ deg, where results are not very sensitive to the mass ratio.

The light curves were modelled by means of the BINARY MAKER 3 software (http://www.binarymaker.com/). Linear limb darkening and gravity darkening coefficients were taken from Claret & Bloemen (2011). The results are in Figs 6 and 7 which, respectively, show the model fits and the physical configuration. The same model parameters were used for all four light curves – these are listed in Table 2. Adding a dark (temperature 96 per cent of the stellar temperature) star-spot improves the fit for three of the four filters:

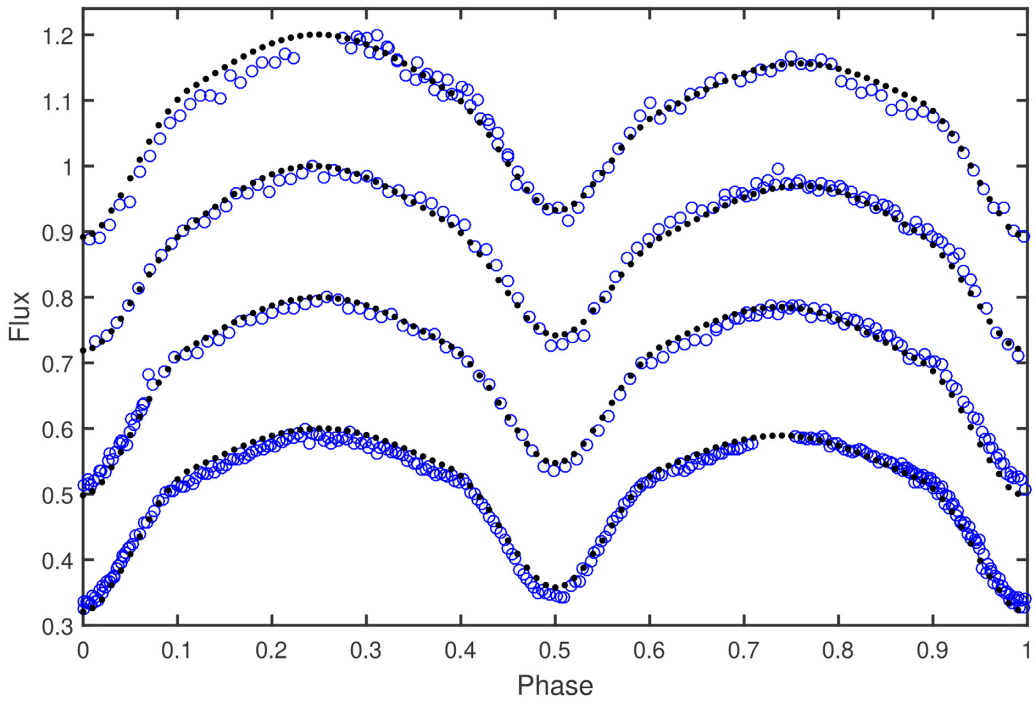

Figure 6. The model of Table 2 (black dots) fitted to the observations (open blue circles) of ATO J199.6731−31.7189. From top to bottom *B*, *V*, *R*, and *I*. The vertical scale is accurate, but zeropoints are arbitrary.

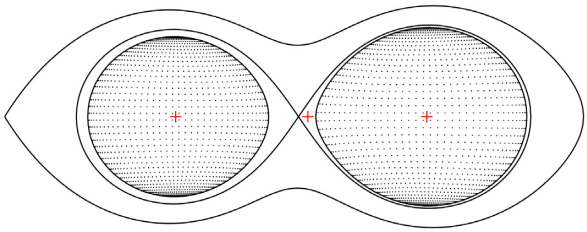

Figure 7. The stellar, and inner and outer Lagrangian surfaces implied by the Table 2 parameters of ATO J199.6731−31.7189.

Table 2. Parameters of a model which provides reasonable fits to the observations of ATO J199.6731−31.7189.

Parameter	Value
T_1	3200 K
T_2	3100 K
i	69°
M_1/M_2	0.9
Fillout 1	−0.07
Fillout 2	−0.04
Parameters of spot (on hotter star):	
Latitude	70°
Longitude	100°
Radius	25°
Temperature	3070 K

the sum of squared residuals (*SSR*) is decreased by 64 per cent (*B*), 46 per cent (*V*), and 9 per cent (*I*), respectively. For the *R* filter the SSR *increases* by 27 per cent. Given the large improvements in the fits for the *B* and *V* data, the spot is retained. Ideally, a formal hypothesis test should be performed to check whether the additional complexity (4 additional parameters) justifies the inclusion of the star-spot in the model. This is not simple, as three of the parameters (the spot latitude and longitude, and its temperature) are not relevant under the null hypothesis of a zero spot size – see e.g. Hansen (1996) for a discussion of this type of issue. As a second best, the Bayesian Information Criteria

$$BIC = N \log(SSR/N) + K \log(N),$$

(N being the number of measurements, K the number of parameters) of rival models can be compared; models with the smallest *BIC* are preferred. The *BIC* favours the models with spots for *B*, *V*, and *I*.

The modelling results are quite insensitive to the adopted mass ratio, and only weakly dependent on the specific stellar temperatures and star-spot parameters.

4 LB 283

The first mention of this star in the literature was by Luyten & Seyfert (1956), who included it in a list of faint blue stars. Kilkenny et al. (1997) provided a spectroscopic classification (sdB) and *UBV* photometry; their $B - V$ and $U - B$ indices are consistent with the classification as a hot subdwarf star. Many properties of the star are summarized in the exhaustive hot subdwarf catalogue of Geier et al. (2017). Notably, the reddening is given as $E(B - V) = 0.10$ mag, with an error of 0.0024 mag ($A_V = 0.308$ mag). The authors used different colour indices (based, amongst others, on 2MASS, *GALEX*, and APASS photometry) to rule out a possible main-sequence companion to the sdB star. The parallax of LB 283 is 1.554 mas (Gaia Collaboration 2018a), leading to an absolute magnitude of $M_V = 4.33$, which is unremarkable for a hot subdwarf star (e.g. Geier et al. 2019).

Kilkenny et al. (2019) modelled a spectrum of the star and obtained an effective temperature ($T_{\rm eff} = 32000 \pm 2000$) and gravity ($\log g = 5.6 \pm 0.2$). As mentioned in the Introduction, they also modelled the variability of the star as being due to a reflection off a very low mass companion. At $M \sim 0.16\,{\rm M}_\odot$, the secondary star would not be expected to contribute much to the overall radiation, and its presence would therefore not necessarily be discernible from photometric indices.

Periodograms were calculated for all available data sets, with the results given in Table 3. The ideal situation would have been one where significant periodicities across all data sets are identified by some statistical test procedure. In reality, such a technique does not exist: in fact, there is not even a generally applicable methodology applicable to single data sets obtained at irregularly spaced time points. We therefore resort to identifying, for each data set, *all* frequencies which lead to reasonable looking phase plots, and then look for correspondences between frequencies seen in different data sets (bearing in mind aliasing).

At first glance the dominant frequency in Table 3 extracted from the CSS observations is quite different from the rest. However, the second largest peak in that spectrum is at the alias frequency 14.1519 d^{-1}, which is adopted as the definitive value of f_0 (because of the superior CSS time baseline). Also, aliases in the *B* and *R* SAAO data are separated by ∼0.2 d^{-1}; for *B*, $13.55 + 3 \times 0.2 = 14.15$ d^{-1}, and for *R*, $13.96 + 0.2 = 14.16$ d^{-1}, so that these are also consistent with f_0. Aliases of the first harmonic of f_0 is present in the SAAO data for each filter. Note also the close correspondence

Table 3. The results of a periodogram study of various sets of observations of LB 283. The number of observations (N) left after removing outliers, and the time interval spanned (ΔT, in days) are given for each data set. Listed is the frequency f_0 (d^{-1}) corresponding to the most prominent peak, followed by peaks at f_1, f_2, ..., in the residual spectra after pre-whitening by the most prominent one, two, ..., peaks. Amplitudes (in millimagnitudes) of the peaks are given in brackets.

	ATLAS *c*	ATLAS *o*	CSS	SAAO *U*	SAAO *B*	SAAO *V*	SAAO *R*
N	168	116	230	220	89	225	81
ΔT	174	247	2888	6	5	6	5
f_0	14.1519 (31)	14.1521 (36)	15.1546 (35)	14.153 (27)	13.547 (28)	14.152 (32)	13.960 (39)
f_1	4.008 (10)	3.2333 (13)	2.8330 (12)	29.322 (4)	7.340 (9)	5.593 (6)	1.410 (22)
f_2	54.603 (10)		6.0592 (12)	1.983 (4)	25.732 (9)	29.480 (4)	27.081 (6)
f_3			1.7158 (10)	18.743 (2)		16.875 (4)	

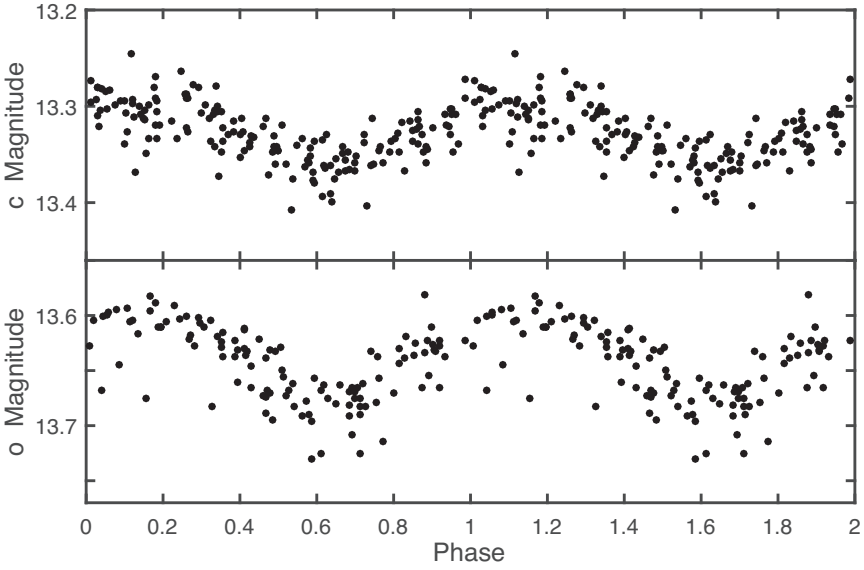

Figure 8. The ATLAS observations of LB 283, phased with a frequency of 14.1519 d^{-1}.

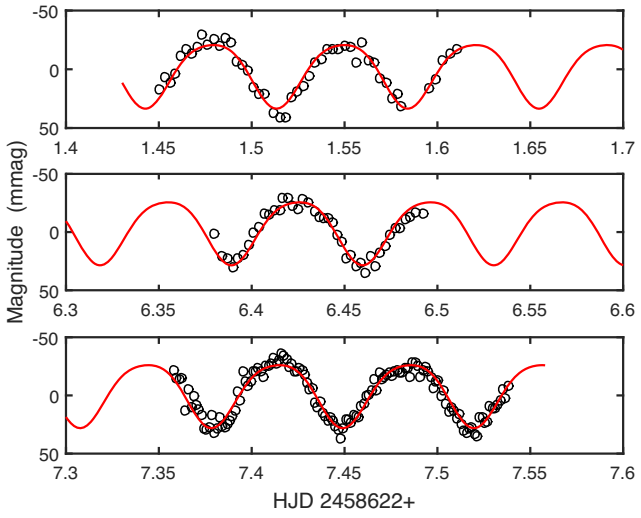

Figure 9. The fit of $f_0 = 14.1519\ d^{-1}$, and its first harmonic, to the SAAO *U*-band observation of LB 283.

between the $f_2 + 2 = 56.60\ d^{-1}$ (ATLAS *c*) and $4f_0 = 56.61\ d^{-1}$. The data are not extensive enough for other frequencies to be considered meaningful. The ATLAS observations can be seen in Fig. 8, phased with a period of $P = 1/14.1519 = 0.070\ 66$ d.

The model

$$y(t) = \mu + A_0 \cos(2\pi\, f_0 t + \phi_1) + A_1 \cos(4\pi\, f_0 t + \phi_2),$$

was fitted to the four SAAO data sets; see Fig. 9 for an illustration. The amplitudes A_0 and A_1 are reported in Table 4. An interpretation is deferred to section 6.

5 *GALEX* J093448.2−251248

This star was originally classified as an O-type subdwarf by Vennes, Kawka & Németh (2011), who derived estimates of its effective temperature and gravity. The classification was changed to sdB by Németh et al. (2012), with a new temperature ($T_{\rm eff} = 34400$ K) and

Table 4. A model for the SAAO photometric observations of LB 283 (see the text). The base frequency is $f_0 = 14.1519\ d^{-1}$. Numbers in brackets give formal uncertainties in the last digit.

Filter	Ampl f_0 (mmag)	Ampl $2f_0$ (mmag)
U	27.0 (5)	4.3(5)
B	27(2)	4(2)
V	32.0(8)	4.2(8)
R	40(2)	8(2)

gravity (log $g = 5.17$). The reddening at the position of the star is $E(B-V) = 0.061$ mag, with extinction $A_V = 0.19$ mag (Schlafly & Finkbeiner 2011). The *Gaia* parallax is 1.10 mas, which together with the APASS measurement $V = 13.09$ implies $M_V = 3.30$.

Results of a spectral analysis of useful available observations of the star are summarized in Table 5. It appears that a frequency close to an integer number of cycles per day is present throughout – 8 or 7 d^{-1} in the ATLAS data, 9 d^{-1} in the CSS observations, and 6 or 7 d^{-1} in the SAAO data. These are evidently aliases. The higher two frequencies can probably be ruled by the HJD 245 8625 SAAO observations (see Fig. 11). On the other hand, phasing of the ATLAS observations with 6 d^{-1} leads to an almost flat light curve, contrasting with the convincing phase plot in Fig. 10. A frequency of 7 d^{-1} is therefore adopted.

The large amplitude (36 mmag) periodicity of ∼1845 d in the CSS data may be due to seasonal variations in the data zero-points; similarly the 1 d period is most likely due to small differences in daily zero-points. There is no sign of the ∼20 min periods (f_1) in the ATLAS data in any of the other sets of observations.

Fitting a sinusoid with frequency 7 d^{-1} to linearly detrended SAAO data and pre-whitening leads to residual spectra which are essentially featureless – largest peaks lie in the range 2.1–3.8 mmags. The results of fitting f_0 to the four data sets can be seen in Table 6, while Fig. 11 illustrates the quality of the fit to the *V* data.

Table 5. As for Table 2, but for *GALEX* J093448.2−251248.

	ATLAS *c*	ATLAS *o*	CSS	SAAO *U*	SAAO *B*	SAAO *V*	SAAO *R*
N	132	163	260		162		
ΔT	508	562	2731		9.0		
f_0	8.000 (23)	6.998 (28)	5.42E-4 (36)	5.987 (19)	5.985 (22)	6.988 (23)	5.980 (25)
f_1	72.84 (9)	71.042 (8)	1.0056 (33)	8.736 (6)	7.385 (5)	1.627 (3)	2.151 (5)
f_2		1.428 (7)	9.0005 (26)	2.814 (4)	2.809 (4)	0.355 (19)	10.059 (5)
f_3			3.9047 (18)	13.85 (3)	18.85(3)	8.827 (3)	17.353 (4)

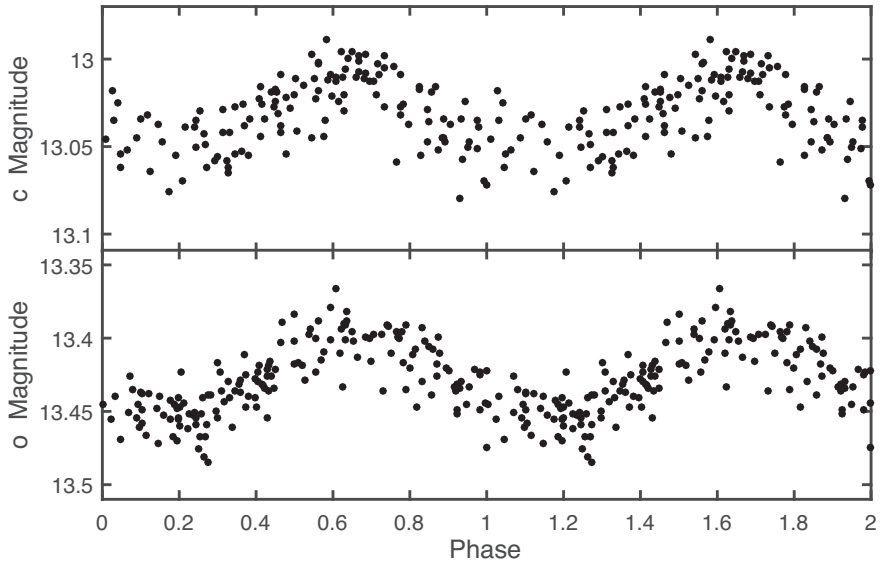

Figure 10. The ATLAS observations of *GALEX* J093448.2−251248, phased with a frequency of 6.9976 d^{-1}.

Table 6. Amplitudes (in millimagnitudes) of single sinusoids with $f = 7$ d^{-1} fitted to the detrended SAAO photometric observations of *GALEX* J093448.2−251248. Numbers in brackets give formal uncertainties in the last digit.

Filter			
U	*B*	*V*	*R*
21.3(9)	22.5(8)	23.2(7)	26.7(9)

6 MODELLING THE SUBDWARF OBSERVATIONS

There is a noteworthy outcome of the analysis above which is largely model-independent: the amplitude of the principal periodicity slightly *increases* with increasing wavelength for both LB 283 and *GALEX* J093448.2−251248. The simplest explanation requires that the sdB star be in a binary system. If the sdB star dominates the light output then variability could be due to reflection off a cool companion. This is now explored in some detail, using simple models.

It is assumed that the only observable optical emission from the secondary star is re-processed radiation from the sdB star. Maxted et al. (2002) derive the rough estimate

$$\frac{T_2}{T_1} \approx \left(\frac{R_1}{\sqrt{2}A}\right)^{1/2}, \quad (2)$$

where it is assumed that *all* the radiation received from the subdwarf star is re-radiated. In equation (2) subscripts '1' and '2', respectively, refer to the sdB star and its companion. The separation A between the two stars is obtainable from Kepler's third law ,

$$A = 4.208 P^{2/3}(M_1 + M_2)^{1/3}, \quad (3)$$

where P is the period in d and other quantities are measured in solar units. It follows from equations (2) and (3) that

$$\frac{T_2}{T_1} \approx 0.410 R_1^{1/2} P^{-1/3}(M_1 + M_2)^{-1/6}. \quad (4)$$

The radius R_1 of the subdwarf star can be calculated from published values of log g:

$$\log\ R_1 = \frac{1}{2}(4.438 + \log\ M_1 - \log\ g_1).$$

Assuming $M_1 \approx 0.5$ (e.g. Heber 2016), and using log $g = 5.6$ (Kilkenny et al. 2019) and log $g = 5.17$ (Németh et al. 2012), $R_1 = 0.19\,R_\odot$ (LB 283) and $R_1 = 0.30\,R_\odot$ (*GALEX* J093448.2−251248) follow. Using periods $P = 0.0707$ and $P = 0.1429$ d (respectively from Tables 4 and 6), and effective temperatures T_1 quoted in sections 4 and 5,

$$T_2 \approx 0.432(M_1 + M_2)^{-1/6} T_1 = 13\,800(M_1 + M_2)^{-1/6}\ \mathrm{K},$$

for LB 283 and

$$T_2 \approx 0.427(M_1 + M_2)^{-1/6} T_1 = 14\,700(M_1 + M_2)^{-1/6}\ \mathrm{K},$$

for *GALEX* J093448.2−251248. If it is furthermore assumed that M_2 is negligible, and again setting $M_1 = 0.5\,M_\odot$, quite similar

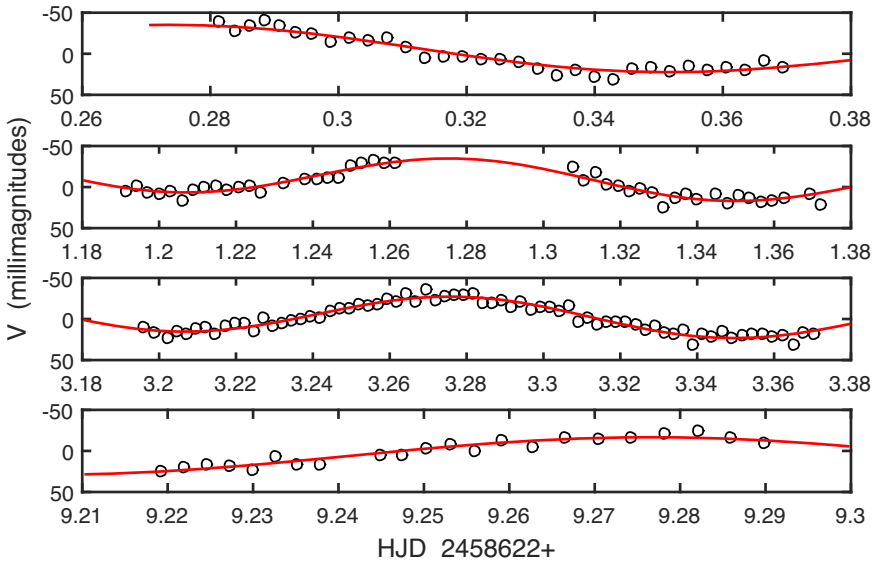

Figure 11. The fit of a sinusoid with $f_0 = 7\ \mathrm{d}^{-1}$ to the detrended SAAO *V*-band observations of *GALEX* J093448.2−251248.

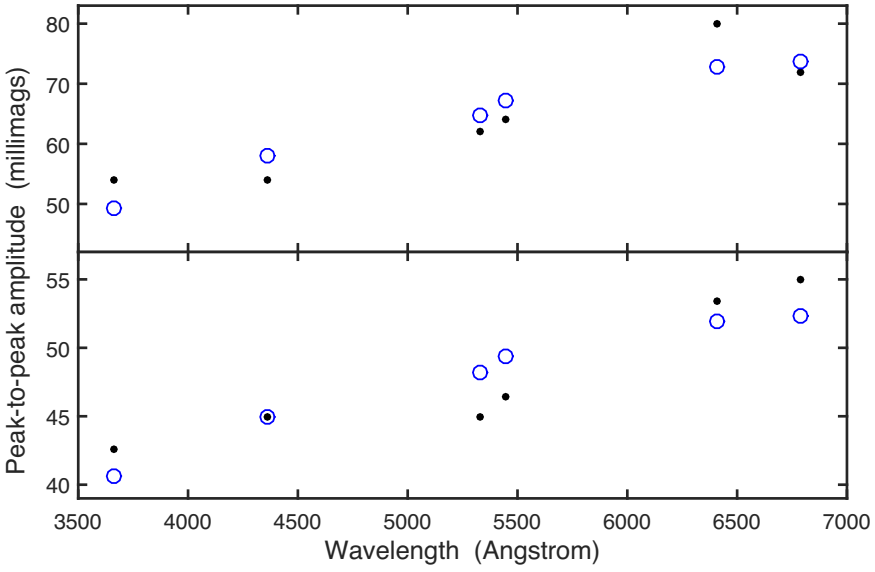

Figure 12. A comparison between predicted (open circles) and observed (solid dots) variability amplitudes of the two sdB stars at different wavelengths (LB 283 top, *GALEX* J093448.2−251248 bottom). From left to right *U*, *B*, *c*, *V*, *R*, and *o*.

temperatures of 15 500 and 16 500 K are obtained for the heated faces of the secondary stars. Note that the dependence of the results on the precise masses is very weak.

A second independent approach makes use of the amplitudes associated with f_0 in Tables 3–6. The amplitude at an effective wavelength λ is described by

$$\Delta m = 2.5 \log_{10} \left(1 + \frac{R_2^2 \mathcal{F}_{2\lambda}}{R_1^2 \mathcal{F}_{1\lambda}} \right),$$

where

$$\mathcal{F}_{j\lambda} = \int_{\lambda_1}^{\lambda_2} \mathcal{T}(\lambda) F_j(\lambda) d\lambda \ .$$

In these equations $\mathcal{F}_{j\lambda}$ is the flux of star j measured at effective wavelength λ, obtainable by weighting the integration of the monochromatic flux $F_j(\lambda)$ by the filter transmission function $\mathcal{T}(\lambda)$.

The simplest is to assume blackbody radiation at temperatures T_1 and T_2, and that is what we do. Filter transmission functions as in Bessell (2005) and Tonry et al. (2018) were used. Theoretical predictions of Δm_U, Δm_B, Δm_V, Δm_R, Δm_c, and Δm_o can be matched to observed values, adjusting the unknowns R_2/R_1 and T_2 to get the best fit. Temperatures T_1 are again taken from the literature.

Results are plotted in Fig. 12. The best parameter values are $R_2/R_1 = 0.46$, $T_2 = 16\ 100$ K (LB 283), and $R_2/R_1 = 0.33$, $T_2 = 20\ 300$ K for *GALEX* J093448.2−251248.

Given the simplicity of the two models the agreement between the two sets of temperatures is reasonable, at least for LB 283. The

Table 7. Physical properties of LB 283 and *GALEX* J093448.2−251248, from the literature (Németh et al. 2012; Kilkenny et al. 2019) and as derived in Section 6. Values of T_2 were estimated by two different methods – see the text for details.

	T_1 (K)	R_1 ($R_\odot$)	$T_2(1)$ (K)	$T_2(2)$ (K)	R_2 ($R_\odot$)
LB 383	32 000	0.19	15 500	16 100	0.087
GAL 0934	34 400	0.30	16 500	20 300	0.11

ratio R_2/R_1 of radii can be used together with the values of R_1 determined above to find $R_2 \sim 0.087\,R_\odot$ (LB 283) and $R_2 \sim 0.11\,R_\odot$ (*GALEX* J093448.2−251248). The LB 283 secondary radius is small for a red dwarf, but within the realm of extremely low mass white dwarfs (ELM WDs; e.g. Tremblay et al. 2015; Bell, Hermes & Kuszlewicz 2018). Inspection of fig. 3 of Bell et al. (2018) suggests $M_2 \sim 0.16\,M_\odot$ – the same as obtained by Kilkenny et al. (2019) by a rather different route.

Physical parameters for LB 283 and *GALEX* J093448.2−251248 derived in this section are collected in Table 7.

7 CONCLUSIONS

To date there is only one known overcontact M-dwarf binary, SDSS J001641−000925 (Davenport et al. 2013). Its component masses correspond to spectral types of M0 and M3, and to the author's knowledge its period is the shortest of any known contact binary – 0.199 d. The preliminary modelling of Section 3 suggests that ATO J199.6731−31.7189 may be in a near-contact, rather than overcontact, configuration. None the less, given that its light curves closely resemble those of contact binaries, the star is clearly worthy of further investigation both because of its period, which is substantially shorter than the oft-quoted 0.2 d limit, and its relatively late spectral type. Davenport et al. (2013) discuss a few other known and candidate M dwarf binaries, only one of which has a period below 0.19 d.

The importance of the study of detached M binaries, on the other hand, has been argued by, for example, Birkby et al. (2012). The primary reason is to help resolve discrepancies between theoretical model predictions and observations. Only a handful of detached or near contact M binaries with periods close to 0.1 d are known (e.g. Nefs et al. 2012; Soszyński et al. 2014). Since ATO J199.6731−31.7189 is quite bright ($V = 15.8$), acquiring radial velocities, and hence establishing accurate component masses and radii, should be relatively easy. This would be useful in view of ongoing studies of radius inflation in short period low mass binaries (e.g. Torres 2013; Cruz et al. 2018). Spectra could also reveal the presence of magnetic fields, often cited as the probable cause of inflated radii in late-type stars (Torres 2013). If, as seems likely, rotation is synchronized with the binary period, $v = 432\,R/R_\odot$ km s^{-1}. Such rapid rotation also favours strong magnetic fields. Finding chromospheric emission lines in either or both component spectra would furthermore support the interpretation of spikes in the light curves of ATO J199.6731−31.7189 as magnetically driven microflares. Spectral lines are bound to be wide – $v \sin i \sim 100$ km s^{-1} if $R/R_\odot \sim 0.26$ and $i \sim 65$ deg.

Clearly more extensive observations are needed to obtain a definitive model for the variability in the two subdwarf stars. The data reported in this paper were obtained at high airmass and under generally poor observing conditions. The frequency analyses of the data also deserve more work. Preliminary simulation studies suggest that it is possible to identify low-amplitude signals by looking for coincidences amongst lesser (i.e. non-significant) peaks in the periodograms of independent data sets. In other words, the usual approach of calculating false alarm probabilities (which often requires unrealistic assumptions) may not be necessary in the present context.

Fortunately, in both the LB283 and *GALEX* analyses only a single frequency (and possibly its first harmonic) is extracted, justified by its presence (or that of an alias) in *all* the data sets. The only other role the frequency analyses played was to make sure that no other signals are overtly present in all or most of the duplicate sets of observations.

The currently most plausible physical model for the two subdwarf stars is that both have faint companions and that the variability is due to reflection off these companions, which could be ELM WDs, very low mass red dwarfs, or brown dwarfs.

Interestingly, although companions with very low masses (below 0.08 $M_\odot$) have been found in a number of sdB binaries (see e.g. Kawka et al. 2015 and Heber 2016), it has rarely – if ever – been suggested that these are ELM WDs. An exception is the speculation by Bell et al. (2019) that *TESS* observations of the hot subdwarf TIC 142875987 are best explained by the presence of an ELM WD, albeit with a mass of 0.3 $M_\odot$. Recent work (Li et al. 2019) on double white dwarf systems suggests the majority of ELM WDs with masses below 0.22 $M_\odot$ are formed by Roche lobe overflow of relatively low mass progenitors ($< 1.45\,M_\odot$), while common envelope ejection produces the more massive ELM WDs. The same two formation channels have been invoked for sdB stars in binary systems – standard references are Han et al. (2002, 2003). The implication is that any sdB + ELM WD binaries would be produced by at least two episodes of considerable mass loss.

The colour–colour plot in Fig. 1 represents data from a very limited area on the sky. Many other interesting ATLAS variables no doubt await further observations.

ACKNOWLEDGEMENTS

Allocation of telescope time by the South African Astronomical Observatory, and the smooth operation of the equipment, are gratefully acknowledged. The paper benefitted from comments by the referee.

REFERENCES

Andrae R. et al., 2018, A&A, 616, 8
Barlow B. N. et al., 2013, MNRAS, 430, 22
Bell K. J., Hermes J. J., Kuszlewicz J. S., 2018, in Castanheira B., ed., 21st European Workshop on White Dwarfs, ASP Conf. Ser., San Francisco
Bell K. J. et al., 2019, Res. Notes Am. Astron. Soc., 3, 81
Bessell M. S., 2005, ARA&A, 43, 293
Birkby J. et al., 2012, MNRAS, 426, 1507
Calcaferro L. M., Córsico A. H., Althaus L. G., 2017, A&A, 607, A33
Chambers K. C. et al., 2016, preprint (arXiv:161205560)
Claret A., Bloemen S., 2011, A&A, 529, A75
Crossfield I. J. M. et al., 2018, ApJS, 239, 5
Cruz P., Diaz M., Birkby J., Barrado D., Sipöcz B., Hodgkin S., 2018, MNRAS, 476, 5253
Cutrie R. M. et al., 2013, VizieR On-line Data Catalog: II/328
Córsico A. H., Althaus L. G., Miller Bertolami M. M., Kepler O., 2019, A&A Rev., 27, 7
Davenport J. R. A. et al., 2013, ApJ, 764, 62
Drake A. J. et al., 2014, ApJS, 213, 9
Finlator K. et al., 2000, AJ, 120, 2615

Gaia Collaboration, 2018a, A&A, 616, A1
Gaia Collaboration, 2018b, A&A, 616, A10
Geier S., Raddi R., Gentile Fusillo N. P., Marsh T. R., 2019, A&A, 621, A38
Geier S., Østensen R. H., Nemeth P., Gentile Fusillo N. P., Gänsicke B. T., Telting J. H., Green E. M., Schaffenroth J., 2017, A&A, 600, A50
Hansen B. E., 1996, Econometrica, 64, 413
Han Z., Podsiadlowski P., Maxted P. F. L., Marsh T. R., 2003, MNRAS, 341, 669
Han Z., Podsiadlowski P., Maxted P. F. L., Marsh T. R., Ivanova N., 2002, MNRAS, 336, 449
Hawley S. L. et al., 2002, AJ, 123, 3409
Heber U., 2016, PASP, 128, 082001
Heinze A. N. et al., 2018, AJ, 156, 241
Henden A., Munari U., 2014, Contrib. Astron. Obs. Skalnaté Pleso, 43, 518
Jiang D., Han Z., Ge H., Yang L., Li L., 2012, MNRAS, 421, 2769
Jiang L., Qian S.-B., Zhang J., Liu N., 2015, PASJ, 67, 118
Kawka A., Vennes S., O'Toole S., Németh P., Burton D., Kotze E., Buckley D. A. H., 2015, MNRAS, 450, 3514
Kilkenny D., O'Donoghue D., Koen C., Lynas-Gray A. E., van Wyk F., 1998, MNRAS, 296, 329
Kilkenny D., O'Donoghue D., Koen C., Stobie R. S., Chen A., 1997, MNRAS, 287, 867
Kilkenny D., Worters H. L., Lynas-Gray A. E., 2019, MNRAS, 485, 4330
Koen C., 2011, MNRAS, 415, 3042
Liu Q.-Y., Yang Y.-L., 2003, Chin. J. Astron. Astrophys., 3, 142
Li Z., Chen X., Chen H.-L., Han Z., 2019, ApJ, 871, 148
Luyten W. J., Seyfert C. K., 1956, AJ, 61, 264
Maxted P. F. L., Marsh T. R., Heber U., Morales-Rueda L., North R. C., Lawson W. A., 2002, MNRAS, 333, 231
Muirhead P. S., Dressing C. D., Mann A. W., Rojas-Ayala B., Lépine S., Paegert M., De Lee N., Oelkers R., 2018, AJ, 155, 180
Napiwotzki R. et al., 2019, preprint (arXiv:1906.10977)
Nefs S. V. et al., 2012, MNRAS, 425, 950
Németh P., Kawka A., Vennes S., 2012, MNRAS, 427, 2180
Paczyński B., Szczygieł D. M., Pilecki B., Pojmański G., 2006, MNRAS, 368, 1311
Pecaut M. J., Mamajek E. E., 2013, ApJS, 208, 9
Pecaut M. J., Mamajek E. E., Bubar E. J., 2012, ApJ, 746, 154
Rucinski S. M., 1993, PASP, 105, 1342
Rucinski S. M., 1997, PASP, 105, 1433
Schechter P. L., Mateo M., Saha A., 1993, PASP, 105, 1342
Schlafly E. F., Finkbeiner D. P., 2011, ApJ, 737, 103
Skrutskie M. F. et al., 2006, AJ, 131, 1163
Soszyński I. et al., 2014, Acta Astron., 64, 1
Stępień K., Gazeas K., 2012, Acta Astron., 65, 153
Tonry J. L. et al., 2018, PASP, 130, 064505
Torres G., 2013, Astron. Nachr., 334, 4
Tremblay P.-E., Gianninas A., Kilic M., Ludwig H.-G., Steffen M., Freytag B., Hermes J. J., 2015, ApJ, 809, 148
Vennes S., Kawka A., Németh P., 2011, MNRAS, 410, 2095
Wang S., Chen X., 2019, ApJ, 877, 116
Wright E. L. et al., 2010, AJ, 140, 1868

This paper has been typeset from a TEX/LATEX file prepared by the author.